International Journal of Satellite Communications and Networking

WILEY

ORIGINAL PAPER OPEN ACCESS

Design and Implementation of Transparent Cross-Polarization Interference Compensation in a Wideband Dual-Polarization Satellite Receiver

Svilen Dimitrov[1] | Vito Dantona[2] | Gerhard Mocker[2]

[1]Satellite Networks Department, German Aerospace Center (DLR), Wessling, Germany | [2]WORK Microwave GmbH, Holzkirchen, Germany

Correspondence: Svilen Dimitrov (svilen.dimitrov@dlr.de)

Received: 11 September 2023 | **Revised:** 24 June 2024 | **Accepted:** 22 July 2024

Funding: This work has been supported by the German Federal Ministry for Education and Research under contract 16KIS1247. Bundesministerium für Bildung und Forschung

Keywords: cross-polarization interference (XPI) | dual-polarization receiver | energy efficiency | higher order modulation | polarization division multiplexing (PDM) | satellite communications | XPI-CLEAR

ABSTRACT

In this paper, simultaneous transmission on two orthogonal antenna polarizations in a polarization division multiplexing (PDM) fashion is studied for wideband satellite communication links using dual-polarization satellite receivers for the purpose of doubling the data rate. In order to mitigate the cross-polarization interference (XPI), a new digital blind and transparent XPI compensation method is proposed, coined as XPI correlation learning estimation and adaptive reduction (XPI-CLEAR). The received signal-to-noise-and-interference ratio (SNIR) and packet-error rate (PER) performance with this non-data-aided and non-decision-directed method is assessed in a comprehensively modelled XPI channel with effects such as depolarization due to atmospheric conditions, imperfect cross-polarization discrimination (XPD) of the antennas at the transmitter and the receiver, memory effects due to frequency selectivity of the XPD, and differential frequency offset (DFO) between the two channels. The application of the XPI-CLEAR method presents considerable energy efficiency improvements for all the studied XPI channel effects, and is particularly beneficial for higher order modulation. A low-complexity hardware implementation with symbol rates up to 500 MBaud validates the XPI-CLEAR method as a practical solution to increase the data rates of the satellite air interface and to achieve the doubling of the throughput of the satellite link by the use of PDM.

1 | Introduction

Satellite communications are an important component of today's information society. Beside the customary application areas, for example, digital satellite television, Earth observation, and professional satellite networks, additional use cases have emerged, such as the global internet access via satellite and backhauling of 5G/6G base stations via satellite as part of nonterrestrial networks (NTN). Recently, an increasing number of satellites have been deployed to provide internet connectivity in remote areas, ships, airplanes, and trains, for example, Ka-Sat 9A of Eutelsat, ViaSat-1, ViaSat-2, ViaSat-3, and Starlink of SpaceX. Nowadays, satellite communications are recognized as a integral part of the 5G/6G communications architecture with the important role of providing global network coverage. For this purpose, in addition to geostationary Earth orbit (GEO) high-throughput satellite (HTS) systems, low Earth orbit (LEO) satellites are becoming increasingly popular, due to the inherent shorter transmission delays and better suitability to low-latency applications.

A number of satellite applications require high data rates over large bandwidths, for example, satellite downlinks for Earth observation, gateway feeder links for direct-to-home internet, and backhauling satellite links for mobile base stations. Due to the

limitation of the available radio frequency (RF) spectrum, polarization division multiplexing (PDM), that is, simultaneous transmission on two orthogonal antenna polarizations, using the same carrier frequency, has the potential to double the data rate of such high-bandwidth communication links. While current multi-beam satellite systems utilize a 4-color reuse scheme with two frequency bands and two polarizations for the user links [1], future multi-beam satellite systems can benefit from PDM to increase the system capacity by using both polarizations in the same beam. Depending on the communication scenario, the PDM setup can be realized either by using dual-polarization antennas at the satellite and the gateway or user terminal or by using two co-located satellites with single-polarization antennas and two single-polarization antennas at the gateway or user terminal. An example of an operational dual-polarization satellite system utilizing PDM technology for Earth observation is WorldView-3 [2].

Because of imperfections of the antennas at the transmitter and the receiver, as well as due to the effects of the atmosphere caused by water droplets and ice crystals, the two polarizations are not completely orthogonal, resulting in cross-polarization interference (XPI). The XPI is higher with the increase of the carrier frequency, for example, in Ku, Ka, and Q/V band, and at lower elevation angles, that is, a longer propagation path through the atmosphere. The increased XPI between the two channels reduces the signal-to-noise-and-interference ratio (SNIR) at the receiver and degrades the performance of the demodulator and decoder. In state-of-the-art LEO satellite systems for Earth observation [1, 3], adaptive coding and modulation (ACM) is employed to adjust the modulation format according to the elevation-dependent XPI and the resulting SNIR conditions during the satellite visibility window. A high XPI is, therefore, a limiting factor for the application of higher-order modulation formats and the achievable data rates. In order to mitigate the effects of this time-variable XPI, an adaptive receiver algorithm performing XPI estimation and compensation is required.

Proprietary solutions have been developed to compensate the XPI at the receiver. Based on an adaptive filter architecture with access to the signals on both polarizations prior to the symbol demapping and decoding stages, an XPI cancellation (XPIC) method has been described in Rossi et al [4]. It can be applied on the signals of the two polarizations either in a symbol-spaced or a fractionally spaced fashion. The adaptive filters for the intended and interfering paths are trained to generate signals used for the XPI cancellation. The training of the filters can be decision-directed and without prior knowledge of pilot symbols, that is, blind, only requiring knowledge of the used modulation format at the receiver. The training can also be data-aided by means of known pilot symbols at the expense of additional signaling overhead. A closely related cross-polarization digital equalization and automatic filtering (XDEAF) method has been presented in Millerioux et al. [5]. An extension to the XPIC method for operation in scenarios with a differential frequency offset (DFO) between the two channels due to, for example, not perfectly synchronized frequency conversion is presented in Kawai [6], including additional electronic components at the expense of higher receiver complexity. While these approaches reduce the XPI, they also increase the computational complexity of the receiver, due to the required training and XPI compensation with multiple filter coefficients, which can be a constraint for the implementation in high-rate hardware devices and applications. Space-time coding and spatial modulation with link adaptation [7, 8] have also been presented for dual-polarized mobile satellite communications [9, 10]. For their successful demodulation, however, these solutions require channel state information at the receiver (CSIR). In the presence of the time-variant XPI, the CSIR can be obtained by means of frequent data-aided channel estimation using known pilot symbols at the expense of additional signaling overhead. In addition, due to the joint preprocessing of the two signals at the transmitter, these solutions have stringent synchronization requirements on the transmitter hardware which can increase the cost of the space segment.

In this paper, a new digital XPI compensation method is proposed, coined as XPI correlation learning estimation and adaptive reduction (XPI-CLEAR) [11]. The digital XPI-CLEAR method is applied in a dual-polarization satellite receiver, simultaneously processing the signal samples on both channels. This non-data-aided and non-decision-directed method uses the correlation between the two received signals for the adaptive estimation and cancellation of the XPI in a blind and transparent fashion. It can be applied in receivers with independent frequency conversion blocks for the two channels, and it can operate in the presence of DFO between the received signals. It has a lower complexity as compared to the filter-based approaches and is therefore suitable for higher rate applications. While the focus of this study is on the use with DVB-S2X [1] and CCSDS [3] waveforms, the XPI-CLEAR method can also be applied with future new radio (NR) waveforms for NTN [12], as long as the signals of the two polarizations have the same bandwidth, the same carrier frequency and the same spectrum shape. The performance of a dual-polarization satellite receiver implementing the XPI-CLEAR method is simulated in terms of received SNIR and packet-error rate (PER), using an XPI channel model with effects such as depolarization due to atmospheric conditions, imperfect cross-polarization discrimination (XPD) of the antennas at the transmitter and the receiver, memory effects due to frequency selectivity of the XPD and DFO between the two channels. The application of the XPI-CLEAR method presents considerable improvements of the received SNIR over the operational range of ACM for all the studied XPI channel effects and is particularly beneficial for higher order modulation. These results closely translate to the energy efficiency improvements conveyed by the PER simulations. A low-complexity hardware implementation with symbol rates up to 500 MBaud validates the XPI-CLEAR method as a practical solution to increase the data rates of the satellite air interface and to achieve the doubling of the throughput of the satellite link by the use of PDM.

The rest of the paper is organized as follows. Section 2 presents the satellite system model, including the transmission chain and the channel modelling. Section 3 describes the XPI-CLEAR method for compensation of the XPI channel. Section 4 presents the performance evaluation results. Section 5 describes the hardware implementation. Finally, Section 6 concludes the paper.

2 | System Model

In a dual-polarization satellite communication system for Earth observation, a satellite or a pair of collocated satellites

transmit message signals over two channels in a PDM fashion to a ground station using a single antenna or a pair of antennas. For example, one channel utilizes a right-hand circular polarization (RHCP), alternatively a vertical polarization (VP), and another channel utilizing a left-hand circular polarization (LHCP), alternatively a horizontal polarization (HP). The imperfect decoupling of the cross-polarization signals at the antenna introduces XPI from one signal into the other. Transmission over this dual-polarization channel with XPI results in a degradation of the performance of the satellite receiver and consequently in a reduction of the achievable data rates. In order to alleviate the issue, a dual-channel receiver can employ XPI compensation, using the locally available information of the XPI within the two received signals. In this section, the transmission chain, the dual-polarization channel model, and a proposed XPI compensation method are presented.

2.1 | Dual-Polarization Satellite Transmission Chain

The block diagram of a dual-polarization satellite communication system with XPI is presented in Figure 1. At the dual-polarization transmitter side, a stream of data bits in each of the two channels are encoded by means of a forward error correction (FEC) scheme and modulated for transmission. In DVB-S2X [1], first, a Bose-Chaudhuri-Hocquenghem (BCH) encoder is applied, followed by an low-density parity check (LDPC) encoder and bit interleaver. The resulting FEC frames are mapped to symbols, using amplitude and phase shift keying (APSK) modulation with constellations up to 256-APSK at the modulator. The modulated symbols are grouped in physical-layer (PL) frames and scrambled by different scrambling sequences in the two channels, in order to ensure the decorrelation of the two signals. The two signals are then oversampled by a chosen oversampling factor and pulse shaped by means of a square root raised cosine filter (SRRCF) to ensure spectrum integrity of the waveform for RF transmission. After digital-to-analog conversion (DAC), the signals are up-converted to the carrier frequency, for example, in the Ka band, and amplified for transmission over one of the orthogonal polarizations, that is, VP/RHCP or HP/LHCP, of a dual-polarization antenna or a pair of single-polarization antennas.

Each transmitted signal is passed through the dual-polarization channel with XPI, including effects such as depolarization due to atmospheric conditions and imperfect XPD of the antennas at the transmitter and the receiver, as well as memory effects due to frequency selectivity of the XPD [1, 3]. The XPD depends on the following contributions [1]: the XPD of the transmitter antenna, the hydrometeor-induced cross-polarization in the atmospheric propagation channel [13], and the XPD of the receiver antenna. The XPI in satellite links for Earth observation [1, 3] is dependent on the elevation of the satellite, and a cumulative XPD of down to 17 dB can be expected for Ka-band links [1].

At the dual-channel receiver of the ground station, the signals of the two polarizations are acquired by a dual-polarization antenna or a pair of single-polarization antennas. The signals are amplified by means of a low-noise amplifier, and they are distorted by additive white Gaussian noise (AWGN). In the following receiver blocks, each signal is down-converted to baseband, and passed through an analog-to-digital converter (ADC). In this paper, an XPI compensation method, elaborated below, is employed to reduce the XPI in the two signals. In the following, after synchronization, matched filtering and downsampling, the received PL frames in each channel are produced which are then descrambled to extract the received symbols. These are then demapped, deinterleaved, and decoded, to obtain the received data bits.

2.2 | XPI Channel Modelling

The block diagram of the dual-polarization channel model with XPI is presented in Figure 2. The signals of the two polarizations consist of two respective streams of digital samples over time. The samples in each of the two streams are stored in buffers to obtain blocks of N samples, represented as row vectors, where $n = 1, \ldots, N$ is the sample index in the currently processed vector, and the buffer size N is an even number. Therefore, the current pair of output signal row vectors of the two polarizations, $\mathbf{p}_1$

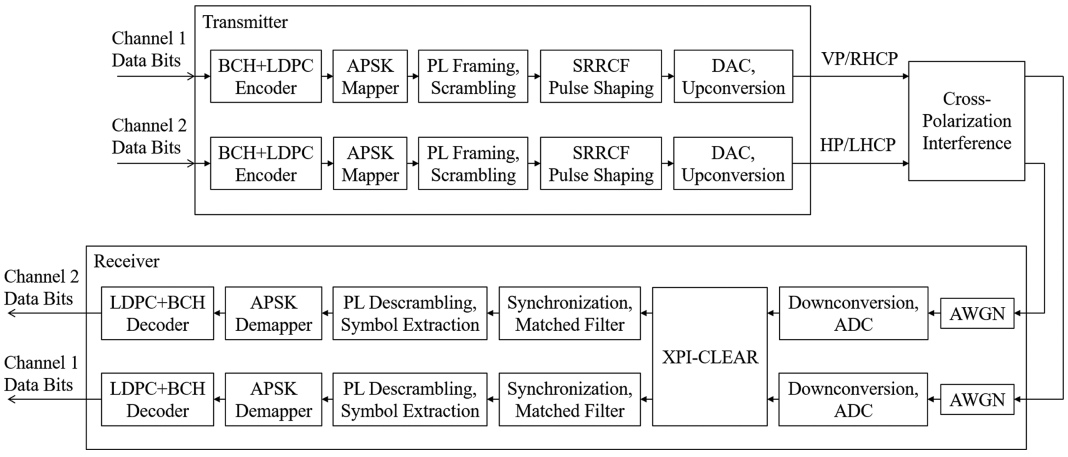

FIGURE 1 | Block diagram of the dual-polarization satellite transmission chain.

and $\mathbf{p}_2$, are expressed in terms of the input signal row vectors, $\mathbf{x}_1$ and $\mathbf{x}_2$, as follows:

$$\begin{aligned}\mathbf{p}_1 = &\sqrt{1-\gamma}\mathbf{x}_1 + \sqrt{\gamma}\exp(i\phi\pi/180)\mathbf{x}_2 \\ &+ \sqrt{\gamma}\exp(i\phi\pi/180)\mathcal{T}\{\mathrm{Conv}\{\mathbf{x}_1, \mathbf{h}\}\} \\ &+ \sqrt{1-\gamma}\mathcal{T}\{\mathrm{Conv}\{\mathbf{x}_2, \mathbf{h}\}\},\end{aligned} \tag{1}$$

$$\begin{aligned}\mathbf{p}_2 = &\sqrt{1-\gamma}\mathbf{x}_2 + \sqrt{\gamma}\exp(i\phi\pi/180)\mathbf{x}_1 \\ &+ \sqrt{\gamma}\exp(i\phi\pi/180)\mathcal{T}\{\mathrm{Conv}\{\mathbf{x}_2, \mathbf{h}\}\} \\ &+ \sqrt{1-\gamma}\mathcal{T}\{\mathrm{Conv}\{\mathbf{x}_1, \mathbf{h}\}\},\end{aligned} \tag{2}$$

where the real-valued linear power-based factor γ is related to the cumulative XPD in the channel as $\mathrm{XPD[dB]} = 10\log_{10}((1-\gamma)/\gamma)$, ϕ is the phase angle in degrees accounting for depolarization due to rain and ice in the atmosphere [14], i is the imaginary unit, $\mathbf{h}$ is the impulse response row vector representing the memory effects due to frequency selectivity of the XPD [15, 16], and $\mathrm{Conv}\{\cdot\}$ is the linear convolution operator, for example, the *conv* function in the MathWorks MATLAB software. Here, the impulse response $\mathbf{h}$ with tap index $l = 1, \ldots, L$ is sampled in accordance with the sampling rate of the signal, the length of the impulse response L is an odd number, and the $\mathcal{T}\{\cdot\}$ operator selects the vector elements from the result of the linear convolution with indices from $(L-1)/2+1$ to $(L-1)/2+N$, corresponding to the N elements of the signal vector. In addition, N is assumed to be much larger than the dominant part of the impulse response, such that this block-based model is a close approximation of a continuous stream. Alternatively, a block convolution with an overlap method can be used to facilitate a continuity between the processed blocks. Examples of impulse responses have been derived from frequency responses published in the literature. The names "conventional," [15] "balanced," [15] and "Iris" [16] are used in the following to identify the impulse responses derived from literature [15, 16]. These are presented in Figure 3 using 2× oversampling in accordance with the sampling rate of the signal.

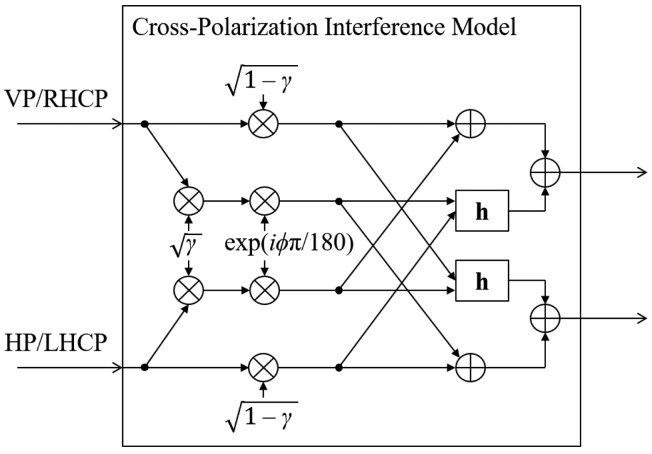

FIGURE 2 | Block diagram of the dual-polarization channel model with XPI.

A common channel effect in the transmission from a LEO satellite to a ground station is the Doppler frequency shift due to the high satellite velocity. For a carrier frequency in Ka band, for example, $f_c = 25$ GHz, and a LEO satellite velocity of 7800 m/s, the Doppler frequency shift amounts to 650 kHz. For a wideband satellite receiver with symbol rates up to 500 MBaud and practical oversampling factors greater or equal to 2.1, aliasing is avoided due to the sufficiently high sampling rates in accordance to the Nyquist theorem. Due to the similar transmission paths of the two signals in the dual-polarization transmission setup, the signals in the two channels are similarly affected by the Doppler frequency shift, and therefore, this effect is insignificant for the XPI compensation. The Doppler frequency shift is then compensated in the subsequent synchronization block of the receiver.

However, when using two independent frequency converters with two independent voltage-controlled oscillators (VCOs) for the downconversion of the two channels, a DFO between the two received signals can be introduced due to VCO instabilities. The DFO can be computed as the product of the carrier frequency, f_c, and the differential sensitivity of the two VCOs in the two channels, S_{VCO}, as follows: $f_{\mathrm{DFO}} = f_c S_{\mathrm{VCO}}$. For example, a DFO of 500 kHz can be expected in a Ka-band satellite system for Earth observation using a 25-GHz carrier frequency and a typical differential sensitivity of the VCOs of 20 ppm. When using sampling rates, f_s, greater or equal to twice the sum of the symbol rate, B_s, and the DFO, the effect of the DFO can be modelled as an elementwise multiplication of the samples of one of the received signals with a rotating complex

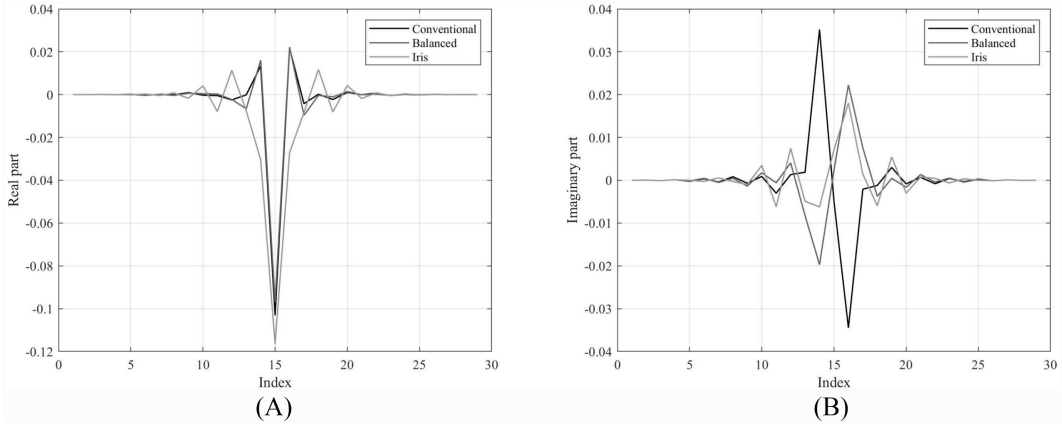

FIGURE 3 | Complex-valued impulse response in the XPI model.

exponential with increment of $360f_{DFO}/f_s$ degrees per sample. As a result, the oversampling factor, η, and the sampling rate, $f_s = \eta B_s$, for a given symbol rate, B_s, can be chosen in accordance with the following inequality: $\eta B_s \geq 2(B_s + f_{DFO})$. For a standard system without an XPI compensation block, the DFO is compensated in the synchronization block. However, as the DFO modifies the information of the XPI contained in each channel, it needs to be considered in the design of XPI compensation techniques.

3 | XPI-CLEAR: A Transparent and Adaptive XPI Compensation

In this paper, a new digital XPI compensation method, coined as XPI-CLEAR, is presented as part of a dual-channel satellite receiver which simultaneously processes the data transmitted on the two polarizations. Having local access to the signals on both channels, the XPI-CLEAR method is input by the oversampled signals of the two polarizations after the ADC stages. Equal path lengths in terms of, for example, cables or copper traces between the receiver antenna and the digital electronics in the two channels are required to avoid differential timing offset between the two signals over this portion of the transmission chain. In addition, two equal synchronous sampling clocks are assumed to drive the two ADCs, which is readily achievable due to colocation of the digital processing electronics, and sampling rates greater or equal to the Nyquist rate are required, which is a common premise in RF communication systems. In the presence of DFO between the two channels in the case when two independent frequency down-conversion blocks are used, the sampling rate has to be sufficiently larger than the Nyquist rate to accommodate the DFO. The XPI-CLEAR block performs estimation and cancellation of the XPI in a transparent and adaptive fashion, concurrently using the signal samples on both channels. The processed signal samples of the two channels are output and respectively fed to the subsequent receiver stages, preserving all structural signal properties.

The oversampled signals of the two polarizations, received after the corresponding ADCs and including the AWGN, can be expressed as follows:

$$\mathbf{y}_1 = \mathbf{p}_1 + \mathbf{w}_1, \tag{3}$$

$$\mathbf{y}_2 = \mathbf{p}_2 + \mathbf{w}_2, \tag{4}$$

where the noise samples, $\mathbf{w}_1$ and $\mathbf{w}_2$, are assumed as independent and identically distributed (i.i.d.) over the sampled bandwidth of ηB_s. Using only the two received sample streams and the knowledge of the oversampling factor used at the two ADCs, the proposed XPI-CLEAR method employs the following complex-valued cross factor between the received signals of the two polarizations [11]:

$$\xi = \mathcal{G}\left\{ \frac{E\left[y_1[n]y_2^*[n]\right]}{E\left[p_1[n]p_1^*[n]\right] + E\left[p_2[n]p_2^*[n]\right]} \right\}, \tag{5}$$

where $E[\,\cdot\,]$ denotes expectation, $(\cdot)^*$ is the complex conjugation operator, and the $\mathcal{G}\{\,\cdot\,\}$ operator applies the following function to the real and imaginary parts of its argument: $g(x) = \text{Real}\left[\left(1 - \sqrt{1-4x^2}\right)/(2x)\right]$. The estimates of the power levels of the noiseless part of the two received signals, $E\left[p_1[n]p_1^*[n]\right]$ and $E\left[p_2[n]p_2^*[n]\right]$, can be obtained from the received signal samples as follows [11]:

$$E\left[p_1[n]p_1^*[n]\right] = E\left[y_{1,\text{odd}}[k]y_{1,\text{even}}^*[k]\right]\alpha, \tag{6}$$

$$E\left[p_2[n]p_2^*[n]\right] = E\left[y_{2,\text{odd}}[k]y_{2,\text{even}}^*[k]\right]\alpha, \tag{7}$$

where the independent noise samples in the odd and even received signal samples are averaged out, $k = 1, \ldots, N/2$, and α denotes the sampling correction factor which is evaluated by means of a numerical simulation of the signals. For a time-division multiplexing (TDM) transmission with SRRCF pulse shaping with roll-off factors between 5% and 35%, which is the case in the majority of satellite communication standards, the sampling correction factor, α, as a function of the oversampling factor, η, is depicted in Figure 4, and a set of values for the corresponding sampling look-up table (LUT) are presented in Table 1. The sampling correction factor is a real-valued number greater or equal to 1, and it converges to 1 for very large oversampling factors.

The complex-valued cross factor is used in conjunction with the two received signals, $\mathbf{y}_1$ and $\mathbf{y}_2$, to compute estimates of the XPI in the two channels as $\xi\mathbf{y}_2$ and $\xi^*\mathbf{y}_1$, respectively. The XPI cancellation is performed as the elementwise subtraction of the XPI estimates from the corresponding received signals, in order to produce the output signal samples of the XPI-CLEAR algorithm as follows [11]:

$$\mathbf{y}_{1,\text{out}} = \mathbf{y}_1 - \xi\mathbf{y}_2, \tag{8}$$

$$\mathbf{y}_{2,\text{out}} = \mathbf{y}_2 - \xi^*\mathbf{y}_1. \tag{9}$$

After the current pair of received signal vectors has been processed and output, the next pair of vectors of buffered received

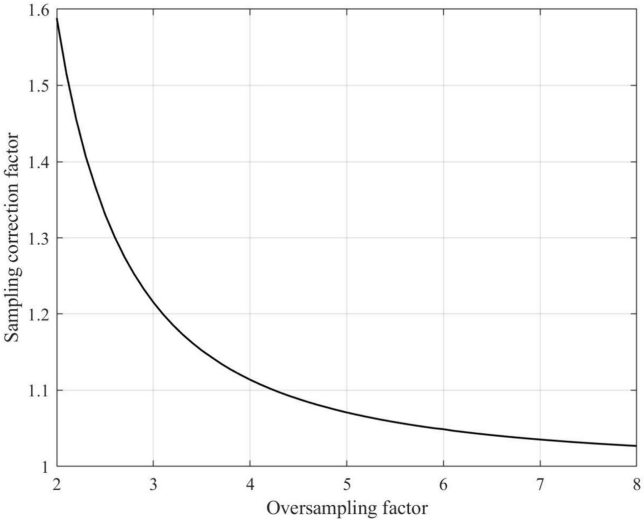

FIGURE 4 | Sampling correction factor as a function of the oversampling factor.

TABLE 1 | LUT for the values of the sampling correction factor as a function of the oversampling factor.

Oversampling factor	Sampling correction factor	Oversampling factor	Sampling correction factor
2	1.5885	3	1.2153
2.1	1.5153	3.2	1.1858
2.2	1.4562	3.4	1.1624
2.3	1.4068	3.6	1.1434
2.4	1.3667	3.8	1.1272
2.5	1.3309	4	1.1138
2.6	1.3009	5	1.0709
2.7	1.275	6	1.0488
2.8	1.2525	7	1.0353
2.9	1.2328	8	1.0269

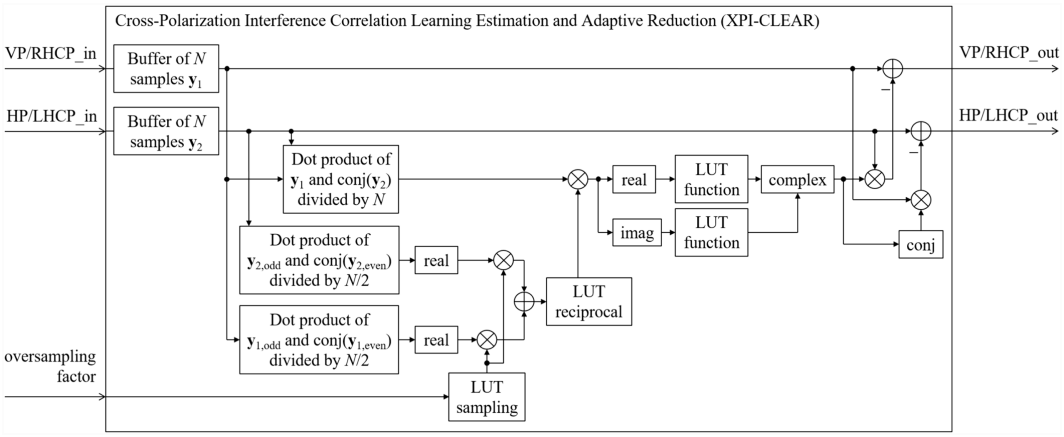

FIGURE 5 | Block diagram of the proposed XPI-CLEAR method.

signal samples is taken, the next cross factor is computed according to (5), and it is used in the XPI cancellation in (8) and (9) to produce the next pair of output vectors of the XPI-CLEAR algorithm.

A practical block diagram for the hardware implementation of the XPI-CLEAR method is presented in Figure 5. As input, the XPI-CLEAR block takes the samples of the oversampled signals of the two polarizations received after the corresponding ADCs. Without loss of generality, complex-valued signals are implied throughout the description, unless otherwise stated, and the separation in in-phase (I) and quadrature (Q) components is considered straightforward. No previous knowledge of the power level or level scaling is required for the signals of the two polarizations. In addition, the oversampling factor, η, used at both ADCs of the two channels is also provided as input. Each received signal of the two polarizations is respectively buffered, in order to construct two row vectors of consecutive samples, $\mathbf{y}_1$ and $\mathbf{y}_2$ with length N, an even number, which are indexed from 1 to N. The elements of the two vectors are used to compute the dot product between the elements of the first vector, $\mathbf{y}_1$, and the complex conjugate of the elements of the second vector, $\text{conj}(\mathbf{y}_2)$. The result is divided by N. In addition, the elements of the first vector, $\mathbf{y}_1$, are also used to compute the dot product between the elements with an odd index, $\mathbf{y}_{1,\text{odd}}$, and the complex conjugate of the elements with an even index, $\text{conj}(\mathbf{y}_{1,\text{even}})$. The result is divided by $N/2$. The elements of the second vector, $\mathbf{y}_2$, are also used to compute the dot product between the elements with an odd index, $\mathbf{y}_{2,\text{odd}}$, and the complex conjugate of the elements with an even index, $\text{conj}(\mathbf{y}_{2,\text{even}})$. The result is also divided by $N/2$. The real parts of the results of the normalized dot product operations with the odd and even elements of each vector are taken, then multiplied by the sampling correction factor, α, and added together. The result of the latter addition is passed through a LUT for the reciprocal function $f(x) = 1/x$, and it is then multiplied with the result of the dot product operations involving the elements of the two vectors. The real and imaginary parts of the result are separately passed through a LUT for the function $g(x) = \text{Real}\left[\left(1 - \sqrt{1-4x^2}\right)/(2x)\right]$. The two results are then respectively combined to form the complex-valued cross factor, ξ. The cross factor is then multiplied with the samples of the

second vector, $\mathbf{y}_2$, to compute an estimate of the XPI in the first vector, $\mathbf{y}_1$, and the result is elementwise subtracted from the samples in the first vector, $\mathbf{y}_1$, to perform the XPI cancellation. The cross factor is also conjugated, then multiplied with the samples of the first vector, $\mathbf{y}_1$, and the result is elementwise subtracted from the samples in the second vector, $\mathbf{y}_2$. The vectors of the two channels after XPI cancellation, $\mathbf{y}_{1,\text{out}}$ and $\mathbf{y}_{2,\text{out}}$, are then provided as the output of the XPI-CLEAR block.

The size of the vectors $\mathbf{y}_1$ and $\mathbf{y}_2$, N, can be selected sufficiently large to provide AWGN averaging, for example, larger than 200 samples. In the case when two independent frequency converters are used for the two polarizations and there is a DFO between the two channels, the upper limit of the vector size, N, can be determined using the DFO, f_{DFO}, and the sampling rate, f_s, as $0.25 f_s/f_{\text{DFO}}$. As a result, the following inequality can be used as a guideline: $200 \leq N \leq 0.25 f_s/f_{\text{DFO}}$.

4 | Performance Evaluation

The performance of a dual-polarization satellite receiver with the XPI-CLEAR method has been evaluated in a PDM satellite downlink transmission for Earth observation in accordance with the DVB-S2X standard [1], using a two orthogonal polarizations, LHCP and RHCP, at a carrier frequency of 25 GHz in Ka band. For the data transmission in each of the two channels, a single-carrier TDM scheme with a symbol rate of 500 MBaud and a carrier roll-off of 20% in conjunction with an oversampling factor of 2, resulting in a sampling rate of 1 Gsps, is assumed. A signal waveform consisting of 100 physical layer (PL) frames is employed in each channel, where each PL frame consists of 10,800 data symbols from a 16-APSK modulation format according to a 4/5-rate LDPC code. For the operation of the XPI-CLEAR method, the vector length is setup to $N = 500$. The performance is evaluated in terms of the carrier-to-interference ratio (C/I) and the carrier-to-noise-and-interference ratio $C/(N+I)$ at the received constellation as a function of the ratio between the energy per symbol and the noise power spectral density E_s/N_0 for a variation of the parameters of the dual-polarization channel with XPI from Figure 2 over their relevant dynamic range in the following scenarios:

- XPD values of 10, 15, and 20 dB. While an XPD of 17 dB can be expected in Ka band [1], the performance of the XPI-CLEAR method is evaluated for XPD values down to 10 dB. This range also corresponds to the relevant range of switching thresholds for ACM with higher order modulation formats.
- Phase angles of 15°, 30°, and 45°, corresponding to the range of values of the depolarization phase angle due to rain and ice in the atmosphere up to 45° [1].
- DFO angle increments of 0.06°, 0.12°, and 0.18° per sample. These values correspond to DFOs of 166, 333, and 500 kHz, respectively, for a carrier frequency of 25 GHz and a sampling rate of 1 Gsps.
- Conventional [15], balanced [15], and Iris [16] impulse responses in the channel model with XPI.

4.1 | Effect of the XPD

In the first scenario, the performance of the dual-polarization satellite receiver with the XPI-CLEAR method has been evaluated for XPD values of 10, 15, and 20 dB, in order to assess the impact of variability of the XPD, for example, due to changing elevation angles during a LEO satellite flight. For the sake of clarity, a higher XPD corresponds to a lower XPI, which in turn translates to a higher C/I. The resulting C/I and $C/(N+I)$ at the received constellation as a function of the E_s/N_0 is presented in Figure 6. It should be noted that very similar performance curves resulted from tests with any modulation orders from QPSK up to 256-APSK, since the XPI-CLEAR method is transparent to the used modulation format.

The degradation of the C/I for E_s/N_0 values lower than approximately 6 dB results in only a minor degradation of the $C/(N+I)$, while the improvement of the C/I for E_s/N_0 values greater than approximately 6 dB results in a significant improvement of the $C/(N+I)$. Since the $C/(N+I)$ at the received constellation is the metric which determines the PER performance of the receiver, the degradation for $C/(N+I)$ values lower than 5 dB when using the XPI-CLEAR method is less than 1 dB for a very low XPD of 10 dB, and it is negligible for

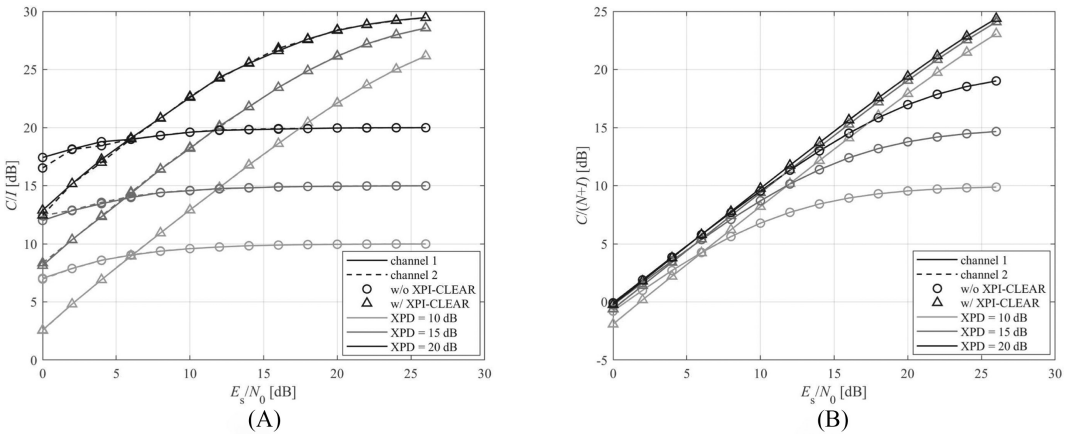

FIGURE 6 | Comparison of the received power ratios as a function of E_s/N_0 for XPD values of 10, 15, and 20 dB.

practical XPD values above 15 dB, therefore, resulting in negligible PER degradation of the receiver in this range. However, the improvements for $C/(N+I)$ values greater than 5 dB are considerable and up to 13.2 dB in the presented scenario. As a result, for lower order modulation formats such as QPSK and 8-PSK which operate in the region of $C/(N+I)$ values lower than 5 dB, only a minor performance degradation less than 1 dB for very low XPD of 10 dB is expected, while the degradation for practical XPD values above 15 dB is negligible. For higher-order modulation formats such as 16-APSK, 32-APSK, and 64-APSK, which require $C/(N+I)$ values greater than 5, to meet the PER target, significant performance improvements are expected. These results justify the suitability of the XPI-CLEAR method for application with ACM.

The gains of the C/I at midrange E_s/N_0 of 14 dB are 6.9, 6.9, and 5.7 dB for XPD values of 10, 15, and 20 dB, respectively. These increase to 16.2, 13.6, and 9.5 dB at higher E_s/N_0 of 26 dB. The gains of the $C/(N+I)$ at midrange E_s/N_0 of 14 dB are 3.7, 1.9, and 0.7 dB. These increase to 13.2, 9.4, and 5.4 dB at higher E_s/N_0 of 26 dB. The XPI-CLEAR method enables the use of the simulated 4/5-rate 16-APSK modulation at an XPD of 10 dB, since it reaches the required $C/(N+I)$ of 11 dB to meet the PER target, and gains of at least 1.8 and 0.4 dB in terms of the required E_s/N_0 are presented for practical XPD values of 15 and 20 dB, respectively.

4.2 | Effect of the Phase Angle

In the second scenario, the performance of the dual-polarization satellite receiver with the XPI-CLEAR method has been evaluated for a practical XPD of 15 dB and phase angles of 15°, 30°, and 45°, in order to assess the impact of depolarization due to atmospheric conditions. Here, a phase angle of 45° represents the worst-case value [1]. The C/I and the $C/(N+I)$ at the received constellation are presented as a function of the E_s/N_0 in Figure 7. While this setup has no impact on the performance of a receiver without the XPI-CLEAR method, it shows a dependence of the performance of the XPI-CLEAR method on the phase angle of the XPI.

The gains of the C/I at midrange E_s/N_0 of 14 dB are 5.8, 3.7, and 2 dB for an XPD of 15 dB and phase angles of 15°, 30°, and 45°, respectively. These increase to 9.4, 5.2, and 2.5 dB at higher E_s/N_0 of 26 dB. The gains of the $C/(N+I)$ at midrange E_s/N_0 of 14 dB are 1.8, 1.3, and 0.8 dB. These increase to 7.4, 4.5, and 2.3 dB at higher E_s/N_0 of 26 dB. For the simulated 4/5-rate 16-APSK modulation at $C/(N+I)$ of 11 dB, gains of 1.7, 1.4, and 1 dB, respectively, in terms of the required E_s/N_0 are presented with the application of the XPI-CLEAR method.

4.3 | Effect of the DFO

In the third scenario, the performance of the dual-polarization satellite receiver with the XPI-CLEAR method has been evaluated for a practical XPD of 15 dB and a DFO with phase increments of 0.06°, 0.12°, and 0.18° per sample, in order to assess the impact of DFO between the samples of the two channels. Here, the vector length of $N = 500$ is considered as the upper value of the inequality $200 \le N \le 0.25 f_s/f_{DFO}$, and so it determines the worst-case value of the phase increment of the DFO as 0.18° for a differential sensitivity between the VCOs in the two channels of $S_{VCO} = 20$ ppm and the considered setup parameters. While in a practical system an oversampling factor of 2.1 will be used to prevent aliasing, the performance of the setup in this simulation using an oversampling factor of 2 and modelling the DFO only as a multiplicative exponential with a phase increment per sample without aliasing is considered very close to the performance of the practical system. The C/I and the $C/(N+I)$ at the received constellation are presented as a function of the E_s/N_0 in Figure 8. While this setup has no impact on the performance of a receiver without the XPI-CLEAR method, since the DFO is compensated in the synchronization block, it shows a dependence of the performance of the XPI-CLEAR method on the phase increment of the DFO.

The gains of the C/I at midrange E_s/N_0 of 14 dB are 6.6, 5.6, and 4.4 dB for an XPD of 15 dB and a DFO with phase increments of 0.06°, 0.12°, and 0.18° per sample, respectively. These increase to 11.7, 8.6, and 6.1 dB at higher E_s/N_0 of 26 dB. The gains of the $C/(N+I)$ at midrange E_s/N_0 of 14 dB are 1.9, 1.7 and 1.5 dB. These increase to 8.7, 7, and 5.2 dB at higher E_s/N_0 of 26 dB. For the simulated 4/5-rate 16-APSK modulation at $C/(N+I)$ of 11 dB, gains of 1.7, 1.6, and 1.5 dB, respectively, in terms of the required E_s/N_0 are presented with the application of the XPI-CLEAR method.

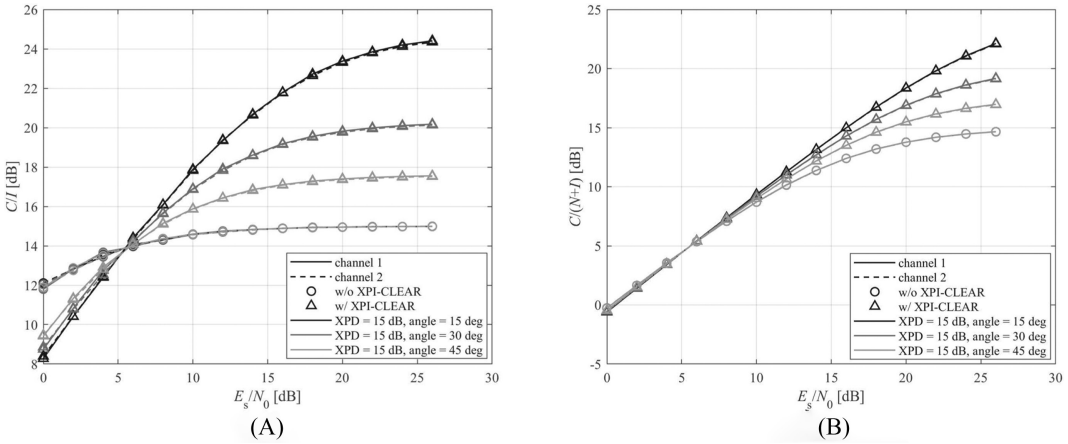

(A) (B)

FIGURE 7 | Comparison of the received power ratios as a function of E_s/N_0 for an XPD of 15 dB and phase angles of 15°, 30°, and 45°.

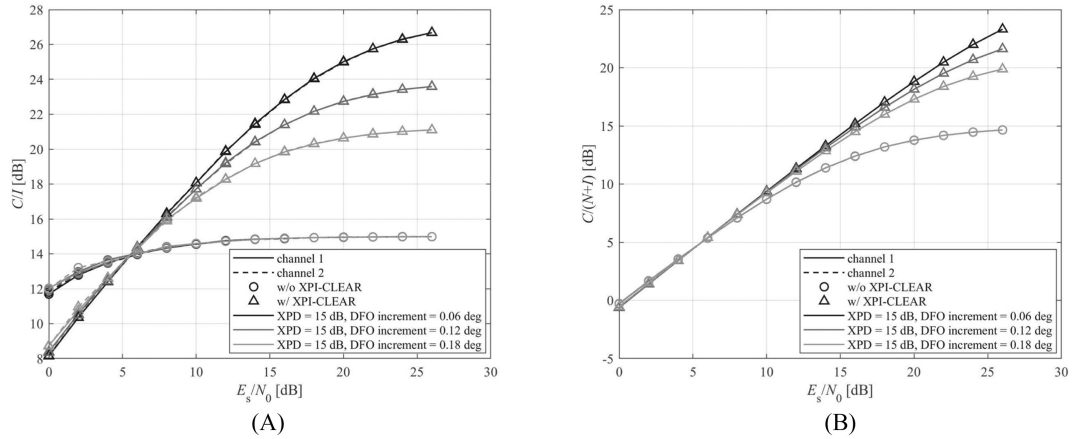

FIGURE 8 | Comparison of the received power ratios as a function of E_s/N_0 for an XPD of 15 dB and a DFO with phase increments of 0.06°, 0.12°, and 0.18°.

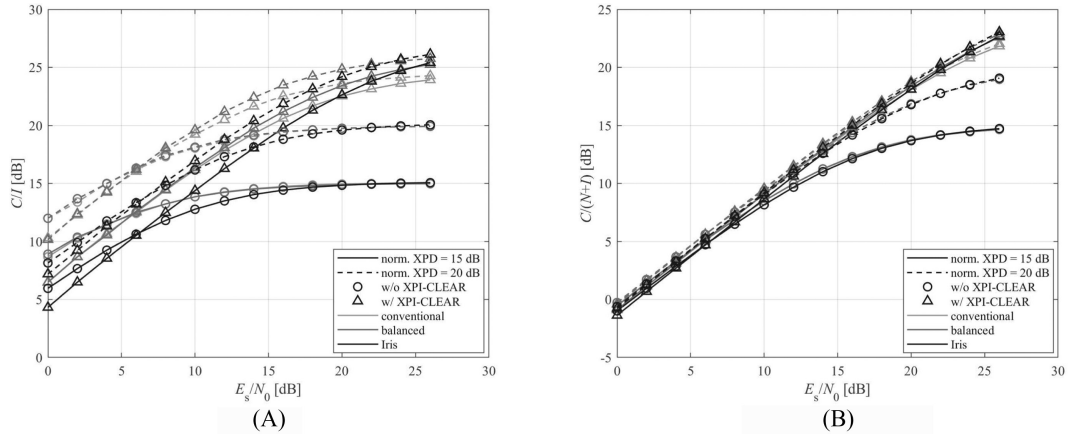

FIGURE 9 | Comparison of the received power ratios as a function of E_s/N_0 for normalized XPD values of 15 and 20 dB and conventional, balanced, and Iris impulse responses in the XPI model.

4.4 | Memory Effects

In the forth scenario, the performance of the dual-polarization satellite receiver with the XPI-CLEAR method has been evaluated for conventional, balanced and Iris impulse responses in the XPI model, in order to assess the impact of memory effects due to frequency selectivity of the XPD, at practical lower and higher normalized XPD values of 15 and 20 dB. Since the impulse responses modify the C/I away from the value set by the XPD-related paremeter γ for a receiver without the XPI-CLEAR method, this parameter has been adjusted such that the C/I converges to a desired normalized XPD for all three examples of impulse responses, in order to only focus on the memory effects. The C/I and the $C/(N+I)$ at the received constellation are presented as a function of the E_s/N_0 in Figure 9. Similar performance has been observed on both channels.

The gains of the C/I at midrange E_s/N_0 of 14 dB are 4.8, 5.2, and 4 dB for a lower normalized XPD of 15 dB and conventional, balanced, and Iris impulse responses, respectively. These increase to 8.8, 10.3, and 10.3 dB at higher E_s/N_0 of 26 dB. The gains of the $C/(N+I)$ at midrange E_s/N_0 of 14 dB are 1.6, 1.7, and 1.6 dB. These increase to 7.2, 8, and 8 dB at higher E_s/N_0 of 26 dB. For the simulated 4/5-rate 16-APSK modulation at $C/(N+I)$ of 11 dB, gains of 1.6, 1.7, and 1.6 dB, respectively, in terms of the required E_s/N_0 are presented with the application of the XPI-CLEAR method.

The gains of the C/I at midrange E_s/N_0 of 14 dB are 2.5, 3.2, and 2.2 dB for a higher normalized XPD of 20 dB and conventional, balanced, and Iris impulse responses, respectively. These increase to 4.4, 5.8, and 6.1 dB at higher E_s/N_0 of 26 dB. The gains of the $C/(N+I)$ at midrange E_s/N_0 of 14 dB are 0.5, 0.6, and 0.5 dB. These increase to 3.1, 3.9, and 4 dB at higher E_s/N_0 of 26 dB. For the simulated 4/5-rate 16-APSK modulation at $C/(N+I)$ of 11 dB, gains of 0.3, 0.3, and 0.3 dB, respectively, in terms of the required E_s/N_0 are presented with the application of the XPI-CLEAR method.

4.5 | PER

The PER performance of the dual-polarization satellite receiver with the XPI-CLEAR method has also been evaluated in the context of the forth scenario, whereby the balanced impulse response in the XPI model has been used with practical lower

and higher normalized XPD values of 15 and 20 dB. Modulation formats of 16-APSK, 32-APSK, and 64-APSK have been selected in conjunction with a 4/5-rate LDPC code, as well as 128-APSK and 256-APSK with a 3/4-rate LDPC code. The PER performance at the receiver has been evaluated as a function of the E_s/N_0 ratio by means of a Monte Carlo simulation. A high number of long PL frames have been simulated, for example, with up to 10^6 packets per simulation point, resulting in sufficient convergence of the statistics down to a PER of 10^{-3}.

The PER performance results are presented in Figure 10. In addition, the E_s/N_0 requirements at PER of 10^{-3} of the selected modulation formats are summarized in Table 2. Without the application of the XPI-CLEAR method, the higher modulation orders of 64-APSK, 128-APSK, and 256-APSK are not applicable at the lower normalized XPD of 15 dB, since the PER saturates above the PER target. With the application of the XPI-CLEAR method in this severe case, these modulation formats are enabled at manageable E_s/N_0 requirements within 1.27 to 2.06 dB of the AWGN only channel. In addition, gains of 1.75 and 4.47 dB are presented for 16-APSK and 32-APSK, respectively. At the higher normalized XPD of 20 dB, gains of 0.38, 0.66, 1.28, 3.06, and 7.99 dB in terms of the required E_s/N_0 are achieved for 16-APSK, 32-APSK, 64-APSK, 128-APSK, and 256-APSK, respectively, with the application of the XPI-CLEAR method. All the E_s/N_0 requirements and the respective gains have shown to be very close to the ones derived when setting the $C/(N+I)$ ratio as target in Figure 9. The presented considerable improvements in energy efficiency and the enabled use of higher-order modulation with practical XPD values down to as low as 15 dB show that the proposed XPI-CLEAR method is a practical solution to increase the spectral efficiency of the air interface, translating not only into increased data rates but also achieving the doubling of the throughput of the satellite link by the use of PDM.

5 | Hardware Implementation

The XPI-CLEAR method has been implemented in very high speed integrated circuit hardware description language (VHDL) and realized on a field programmable gate array (FPGA) chip of the AMD Xilinx Ultrascale+ family. The XPI compensation block has been integrated in a wideband dual-polarization satellite receiver of WORK Microwave GmbH. The FPGA realization of the XPI-CLEAR method successfully achieves the targeted symbol rates of up to 500 MBaud. For a vector size of $N = 256$, the implementation requires the following FPGA resources: 1979 LUTs, 3433 flip-flops (FFs), 7 18k and 9 36k memory blocks (BRAMs), and 104 DSP48E2 digital signal processing (DSP) slices. These resources and the achieved symbol rates reflect the low computational complexity of the XPI-CLEAR method and justify its suitability for very high rate applications.

The block diagram of the hardware implementation of the dual-polarization satellite transmission chain, including a pair of modulators and a dual-channel receiver with the XPI-CLEAR

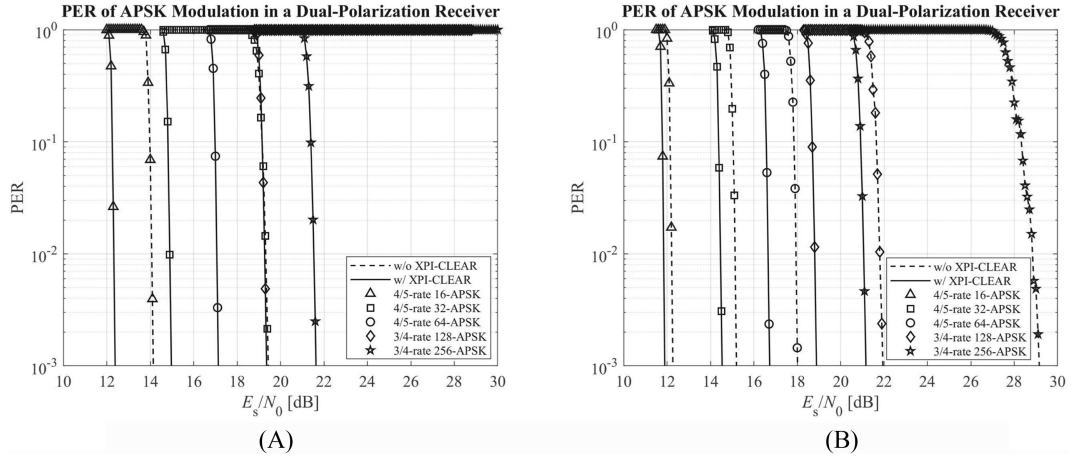

FIGURE 10 | Comparison of the PER as a function of E_s/N_0 for normalized XPD values of 15 and 20 dB and a balanced impulse response in the XPI model.

TABLE 2 | Required E_s/N_0 [dB] at 10^{-3} PER of higher order modulation formats for normalized XPD values of 15 and 20 dB and a balanced impulse response in the XPI model.

Modulation formats		4/5-rate 16-APSK	4/5-rate 32-APSK	4/5-rate 64-APSK	3/4-rate 128-APSK	3/4-rate 256-APSK
AWGN only		11.03	13.64	15.87	17.73	19.57
Norm. XPD of 15 dB	w/o XPI-CLEAR	14.14	19.44	N/A	N/A	N/A
	w/ XPI-CLEAR	12.39	14.97	17.14	19.36	21.63
Norm. XPD of 20 dB	w/o XPI-CLEAR	12.27	15.2	18.01	21.95	29.16
	w/ XPI-CLEAR	11.89	14.54	16.73	18.89	21.17

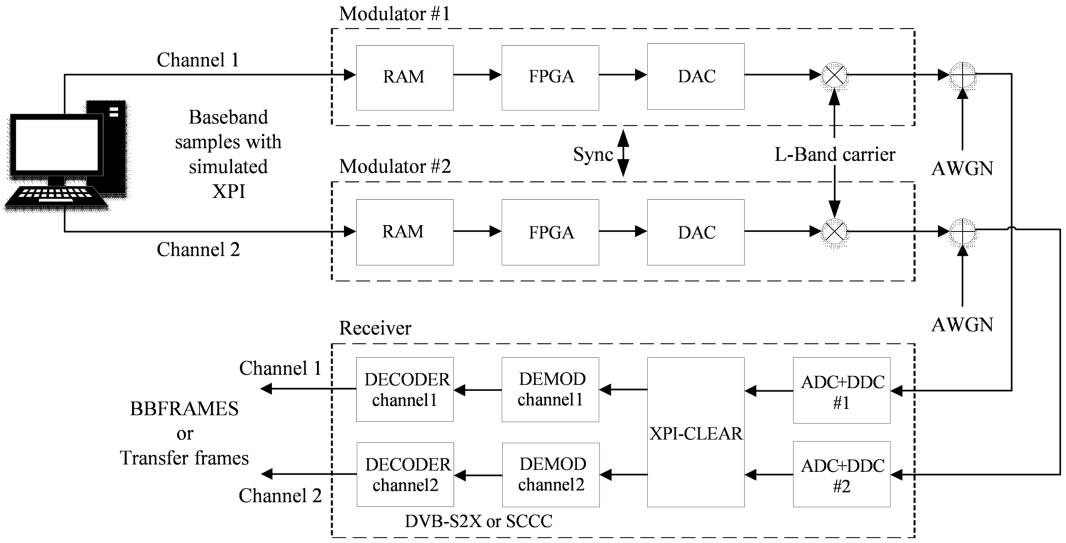

FIGURE 11 | Block diagram of the hardware implementation of the dual-polarization satellite transmission chain, including a pair of modulators and a dual-channel receiver with the XPI-CLEAR method.

block, is presented in Figure 11. Baseband samples with simulated XPI are generated in software on a personal computer (PC) according to the XPI channel model in Figure 2. The samples are stored in the random-access memory (RAM) in a pair of modulators. The samples are passed through the FPGA and the DAC of each modulator and up-converted to an L-band carrier frequency. After adding AWGN, the two signals are input in the two channels of the dual-channel receiver. Each signal is passed through the ADC and digital down-conversion (DDC) blocks, and input in the FPGA implementation block of the XPI-CLEAR method for XPI compensation. The two signals are then demodulated and decoded according the used transmission format, for example, DVB-S2X [1] or serial-concatenated convolutional codes (SCCC) [3]. The output of the dual-channel receiver are either baseband frames (BBFRAMES) or transfer frames.

6 | Conclusion

In this paper, a new digital blind and transparent XPI compensation method, XPI-CLEAR, has been proposed for application in dual-polarization satellite receivers for wideband PDM satellite communication links. The received SNIR and PER performance of the receiver with the XPI-CLEAR method has been assessed in a comprehensively modelled XPI channel with effects such as depolarization due to atmospheric conditions, imperfect XPD of the antennas at the transmitter and the receiver, memory effects due to frequency selectivity of the XPD and DFO between the two channels. The application of the XPI-CLEAR method has shown considerable improvements of the received SNIR over the operational range of ACM for all the studied XPI channel effects, proving particularly beneficial for higher-order modulation. These results have closely translated to the energy efficiency improvements conveyed by the PER simulations. In the studied practical scenario with normalized XPD of 20 dB, the application of the XPI-CLEAR method has presented energy efficiency improvements of 0.4 to 8 dB for the considered modulation orders from 16-APSK to 256-APSK, and it has even enabled the use of 64-APSK, 128-APSK, and 256-APSK for lower normalized XPD of 15 dB. Due to its low computational complexity, the XPI-CLEAR method is suitable for higher-rate applications. A hardware implementation with symbol rates up to 500 MBaud validates the XPI-CLEAR method as a practical solution to increase the data rates of the satellite air interface and to achieve the doubling of the throughput of the satellite link by the use of PDM, translating into higher link throughput and a lower cost per transmitted bit.

Acknowledgements

This work has been supported by the German Federal Ministry for Education and Research under contract 16KIS1247. Responsibility for the contents of this publication lies with the author. (Das diesem Bericht zugrundeliegende Vorhaben wurde mit Mitteln des Bundesministeriums für Bildung und Forschung unter dem Förderkennzeichen 16KIS1247 gefördert. Die Verantwortung für den Inhalt dieser Veröffentlichung liegt beim Autor.)

Conflicts of Interest

The authors declare no conflicts of interest.

Data Availability Statement

Data sharing is not applicable to this article as no new data were created or analyzed in this study.

References

1. "Implementation Guidelines for the Second Generation System for Broadcasting, Interactive Services, News Gathering and Other Broadband Satellite Applications; Part II: S2-Extensions (DVB-S2X), ETSI TR 102 376-2," (2015).

2. T. Kaneko, H. Saito, M. Mita, and Y. Ohikata, "Dual Circularly Polarization X Band 2Gbps Downlink Communication System of Earth Observation Satellite," in *Proc. AIAA/USU Small Satellite Conference (AIAA/USU SSC 2018)*, (Utah, USA, 2018), 1–8.

3. "Flexible Advanced Coding and Modulation Scheme for High Rate Telemetry Applications, CCSDS 131.2-b-1," (2012).

4. L. Rossi, C. Salvaneschi, M. Nava, and A. Miletic, "Interference Erasing System With Independent Receivers, ep1365519b1," (2005).

5. J.-P. Millerioux, E. Peragin, H. Guillon, et al., "Preliminary Definition of a High Performance X-Band Transmitter for Microsatellites," in *Proc. of the 4s Symposium 2012*, (Portoroz, Slovenia, 2012), 1–11.

6. M. Kawai, "Cross Polarization Interference Compensation Method, and Cross Polarization Interference Compensating Device, ep1940061a1," (2008).

7. T. L. Jensen, S. Kant, J. Wehinger, and B. H. Fleury, "Fast Link Adaptation for MIMO OFDM," *IEEE Trans. Veh. Technol.* 59, no. 8 (2010): 3808–3813.

8. P. Yang, Y. Xiao, L. Li, Q. Tang, Y. Yu, and S. Li, "Link Adaptation for Spatial Modulation With Limited Feedback," *IEEE Trans. Veh. Technol.* 61, no. 8 (2012): 3808–3813.

9. M. Sellathurai, P. Guinand, and J. Lodge, "Space-Time Coding in Mobile Satellite Communications Using Dual-Polarized Channels," *IEEE Trans. Veh. Technol.* 55, no. 1 (2006): 188–199.

10. P. Henarejos and A. I. Perez-Neira, "Dual Polarized Modulation and Reception for Next Generation Mobile Satellite Communications," *IEEE Trans. Commun.* 63, no. 10 (2015): 3803–3812.

11. S. Dimitrov, "Method for Receiving Two Digital Signals in a Dual-Polarization Digital Communication System, wo2023/161084a1," (2023).

12. A. Jayaprakash, B. G. Evans, P. Xiao, A. B. Awoseyila, and Y. Zhang, "New Radio Numerology and Waveform Evaluation for Satellite Integration Into 5G Terrestrial Network," in *Proc. IEEE International Conference on Communications (IEEE ICC 2020)*, (Dublin, Ireland, 2020), 1–7.

13. "Propagation Data and Prediction Methods Required for the Design of Earth-Space Telecommunication Systems, ITU-R p.618–13," (2017).

14. W. P. Overstreet and C. W. Bostian, "The Phase of the Crosspolarized Signal Generated by Millimeter Wave Propagation Through Rain, NASA-CR-159894," (1978).

15. H. J. Gould, "Balanced Phase Septum Polarizer, US Patent 4126835," (1978).

16. G. Virone, R. Tascone, O. A. Peverini, G. Addamo, and R. Orta, "Combined-Phase-Shift Waveguide Polarizer," *IEEE Microw. Wireless Compon. Lett.* 18, no. 8 (2008): 509–511.